One-Pot Synthesis of Highly Activated Carbons from Melamine and Terephthaldehyde as Electrodes for High Energy Aqueous Supercapacitors

Noel Díez,[a] Roman Mysyk,[a] Wei Zhang,[ab] Eider Goikolea,[a] Daniel Carriazo *[ab]

[a] CIC EnergiGUNE, Parque Tecnológico de Álava, Albert Einstein 48, 01510 Miñano, Álava, Spain

[b] IKERBASQUE, Basque Foundation for Science, 48013 Bilbao, Spain

e-mail: dcarriazo@cicenergigune.com

Abstract

In this work we report the preparation of porous carbons with very large specific surface areas (over 3000 $m^2\,g^{-1}$) by a simple *all-in-one* route that involves the simultaneous polymerization, carbonization and *in-situ* activation of a mixture of melamine and terephthaldehyde. The influence that different activating agents (KOH and a eutectic mixture of KOH and NaOH) have on the polymerization process and thus the final textural properties of the carbons is also explored. Materials were characterized by X-ray diffractommetry (XRD), Raman spectroscopy, scanning electron microscopy (SEM), transmission electron microscopy (TEM), thermal analysis (TG/DTA) and nitrogen adsorption-desorption at -196ºC. It was found that carbons prepared in the presence of KOH showed a hierarchical multimodal pore-size distribution that combines large micropores and medium-size mesopores while those carbons obtained in the presence of the KOH-NaOH mixture exhibited a narrower distribution within the micropore range and small mesopores. Both materials were tested as electrodes for symmetric supercapacitors using three different aqueous electrolytes, namely 6M KOH, 1M Li_2SO_4 and 5M LiTFSI (lithium bis(trifluoromethanesulfonyl)imide), which allowed their steady cycling at 1.2, 1.8 and 2.2 V, respectively. The different performance between both carbons working in different electrolytes is discussed and related to their textural features. The hierarchical micro-mesoporosity favored a good diffusion of ions when working with LiTFSI, which allows

achieving very high energy densities of 40 Wh kg^{-1} at 0.27 kW kg^{-1}. For moderate requirements

in terms of energy and power density, the same micro/mesoporous material can provide 16

Wh kg^{-1} at 4.3 kW kg^{-1} for 10^4 cycles using Li_2SO_4 as the electrolyte. Finally, both mesopore-

containing and mesopore-free materials can provide very high capacitance values up to 360 F

g^{-1}, a very fast response and excellent cycling performance when working in 6M KOH, being

suitable candidates for high power applications.

Introduction

Electrical double-layer capacitors (EDLCs) are energy storage devices that in terms of energy

and power density are located between conventional capacitors and batteries.[1] EDLCs consists

of two conductive porous electrodes impregnated with an electrolyte and separated by a

membrane that allows ion diffusion but prevents the contact between both electrodes. Energy

is electrostatically stored in EDLCs through the formation of a Helmholtz electrical double layer

between the ions of the electrolyte and the surface of the electrodes, thus enabling its fast

charge-discharge and providing high power density and long cycle life.[2, 3]

Porous carbons are the preferred materials for the fabrication of electrodes for EDLCs due to

their relatively high electronic conductivity, low cost, inertness, high specific surface area and

the possibility to tailor their porosity to fit with the sizes of the electrolyte ions.[4]

Different methods have been reported for the preparation of carbons with high specific

surface area for their potential application as electrodes for supercapacitors.[5, 6] Two-step

processes involving the pyrolysis and activation of biomass wastes[7-12], coals or polymers[13-15]

have been extensively investigated. The main drawback associated to these processes resides

in their limited control over the pore size distribution and the generation of bottlenecks and/or

micropores below 0.6 nm, which are not accessible to the electrolyte ions.

More sophisticated approaches for the synthesis of nanoporous carbons with hierarchical

porosities involve the use of soft or hard templates.[16-19] Despite allowing one to fine tune the

porosity towards specific pore sizes, these are multi-step procedures that require costly precursors, which make them difficult to scale up.[20] Advanced nanostructured carbons such as carbon nanotubes, graphene-based materials or onion-like carbons have been also appointed as potential candidates for the preparation of supercapacitor electrodes.[21-23] However, their moderate surface area as well as high cost and complex synthetic processes also hinder their use in commercial EDLCs.[20]

According to the energy equation, $E = 0.5 \cdot C \cdot V^2$, where C is the capacitance of the cell and V the operational voltage, the energy density of a supercapacitor can be increased in two ways: maximizing the capacitance of each electrode and/or increasing the operational voltage.[24] Capacitance is directly related to the active materials within the electrodes and the operational voltage window is related to the electrochemical stability of the materials and the electrolyte. Organic and ionic liquid electrolytes allow operating voltages up to 2.7V and above, correspondingly, and therefore, are the preferred liquid electrolytes for high energy supercapacitors.[25] Recently, it has also been reported that some aqueous electrolytes such as 1M Li_2SO_4 or 5M LiTFSI can be steadily cycled at 2.2 and 2.4 V, respectively.[26, 27] Although these voltage windows are lower than those allowed by organic or ionic liquid electrolytes, these aqueous systems are still very promising because of their high power density and low cost.[28] Moreover, choosing an aqueous electrolyte instead of an organic or ionic liquid one bypasses the requirement of performing cell assembly under moisture-free environments and the exhaustive drying of carbons prior to their use. Consequently, the complexity and cost of the process, and therefore, the price of the device decrease substantially.[29]

The present work goal was to find a simple procedure for the preparation of high specific surface area carbons with adequate porosity to be used as electrodes in high-voltage aqueous supercapacitors. Within this context, herein we introduce a direct way to obtain very high specific surface area carbons by a one-pot process that involves the *all-in-one* simultaneous polymerization, carbonization and activation of melamine and terephthaldehyde, using two

different activating agents, namely KOH and an eutectic mixture of KOH and NaOH. These carbons exhibited a great performance as electrodes in symmetric EDLC using 6M KOH as well as 1M Li_2SO_4 or 5M LiTFSI aqueous solutions operating at high voltage.

Experimental Section

Synthesis

Two different porous carbons derived from the pyrolysis/activation of melamine and terephthaldehyde were prepared in this work. The first of them, denoted as MTK, was synthesized in the following way: 1.24 g of melamine (M), 1.36 g of terephthaldehyde (T) and 5.0 g of KOH (K) were grinded in an agate mortar and directly heated first at 250ºC for 3h and then at 800ºC for 1h with a heating ramp of 1ºC min^{-1}. The resultant carbonaceous material was washed several times, first with a 3M HCl solution and then with distilled water until the pH was close to 7, and dried at 120ºC overnight. The second sample, hereafter denoted as MTKN, was prepared in a way similar to that described for MTK but a mixture of 2.5 g of KOH and 2.5 g of NaOH (KN) was used as the activating agent.

Physicochemical characterization

X-ray diffraction (XRD) patterns were registered for powdered samples in a Bruker D8 X-ray diffractometer; data were collected at 40 kV and 30 mA using CuKα radiation over 2θ within the range from 5 to 90º at steps of 0.02º and a residence time of 5 seconds. Raman spectra were recorded with a Renishaw spectrometer (Nanonics Multiview 2000) operating with an excitation wave-length of 532 nm. The spectra were acquired with 10 seconds of exposition time of the laser beam to the sample. Scanning electron microscope (SEM) images were acquired in a field emission Quanta 200 FEG microscope from FEI. A Tecnai G2 transmission electron microscope (TEM, FEI) was also employed for microstructural characterization. The powder samples were ultrasonically dispersed in ethanol for 10 mins. Then several drops of the solution were taken on a holey carbon films supported by Cu for TEM characterization.

Thermogravimetric (TG) and differential thermal analysis (DTA) curves were obtained by heating the material with a heating rate of 5 ºC min^{-1} from 50 ºC to 800 ºC under a dynamic atmosphere of argon in a thermogravimetric balance STA 449 F3 Jupiter model from Netzsch. Nitrogen adsorption-desorption isotherms were registered using an ASAP2020 instrument from Micromeritics. Samples were outgassed at 250ºC during 3 h prior to analysis. Specific surface area values were determined using the BET equation within the 0.05-0.2 relative pressure range. The amount of nitrogen adsorbed at a relative pressure of $p/p_0 = 0.95$ was used to determine the total pore volume (V_T). The micropore volume (V_{DR}) was estimated by applying the Dubinin–Radushkevich equation. The mesopore volume (V_{me}) was calculated as the difference between total pore volume and micropore volume. Pore size distributions (PSD) were determined using the non-local density functional theory (NLDFT) method from the nitrogen adsorption branch data assuming a slit-shaped pore model.

*Electrode preparation, cell assembling and electrochemical characterization*

Electrodes were prepared by mixing 90 wt.% of the activated carbon with 5 wt.% of polytetrafluorethylene (PTFE) and 5 wt.% of carbon black in the presence of ethanol. The mixture was kneaded until plasticity, rolled to a thickness of approximately 120 μm and dried at 120ºC overnight. Disk-shaped electrodes of 11 mm in diameter were punched out from the dried film and weighted in a balance.

To perform the electrochemical measurements, two electrodes with similar masses (~2.5 mg cm^{-2}) were assembled in a Swagelok™-type cell placing between them a porous glass fiber (Whatman GFB) membrane, which acted as the separator. The electrodes and the separator were wetted with a couple of drops of the selected aqueous electrolyte (6M KOH, 1M Li_2SO_4 or 5M LiTFSI), and two stainless steel rods were used as current collectors. Cyclic voltammetry (CV), galvanostatic charge-discharge cycling (GC) and electrochemical impedance spectroscopy (EIS) measurements were conducted using a multichannel VMP3 generator from Biologic. The specific capacitance expressed in farads per gram of active material (F g^{-1}) was obtained from

the discharge curve of the galvanostatic plots recorded at different current densities according the equation $C = 2I \cdot t_d / m \cdot V$, where I is the electrical current, V is the usable voltage range once the ohmic drop is substracted, t_d is the discharge time and m is the mass of one electrode. Specific energy (Wh kg^{-1}) and specific power (W kg^{-1}) of the cells were calculated as $E = 1/8\ CV^2$ (1000/3600) and $P = E/t_d$. EIS curves were obtained within a frequency range from 10 mHz to 100 kHz. Relaxation time constants (τ_0) were deduced from the frequency (f_0) at maximum imaginary capacitance C'' (ω).

Results and Discussion

Scheme 1 graphically summarizes the process followed for the preparation of MTK and MTKN activated carbons. This procedure allowed obtaining ca. 320 mg and 110 mg of the final MTK and MTKN carbons after washing, respectively.
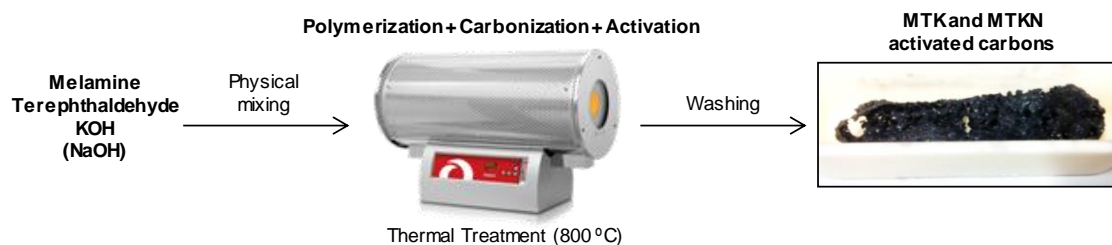
Scheme 1. Synthetic pathway for the preparation of MTK and MTKN activated carbons.

The porous texture of MTK and MTKN was investigated by means of nitrogen physisorption at -196ºC (Figura 1A). It can be noticed that both adsorption-desorption isotherms show a profile in between types I and IV according to the IUPAC classification,[30] which corresponds to materials containing both micro- and mesopores. In the case of MTKN, the higher amount of adsorbed nitrogen at very low relative pressures reveals a higher content of small micropores in this sample. On the other hand, adsorption at high relative pressures discloses the presence of medium-size or big mesopores in MTK as well as their absence in MTKN. The textural

parameters of the porous carbons are summarized in Table 1. Very high BET specific surface areas of ca. 3068 and 3301 $m^2 g^{-1}$ were calculated for MTK and MTKN, respectively (Table 1). The higher specific area measured in MTKN is attributed to a larger volume of micropores (1.00 and 1.13 $cm^3 g^{-1}$ for MTK and MTKN, respectively). Pore size distributions calculated for these samples are depicted in Figure 1B. It can be clearly observed that MTKN sample contains only pores with sizes within the range of 0.5 and 3.5 nm, while MTK carbon contains a bimodal micro-mesoporosity, with pores of 1 to 3 nm in combination with mesopores ranging from 4 to 13 nm.
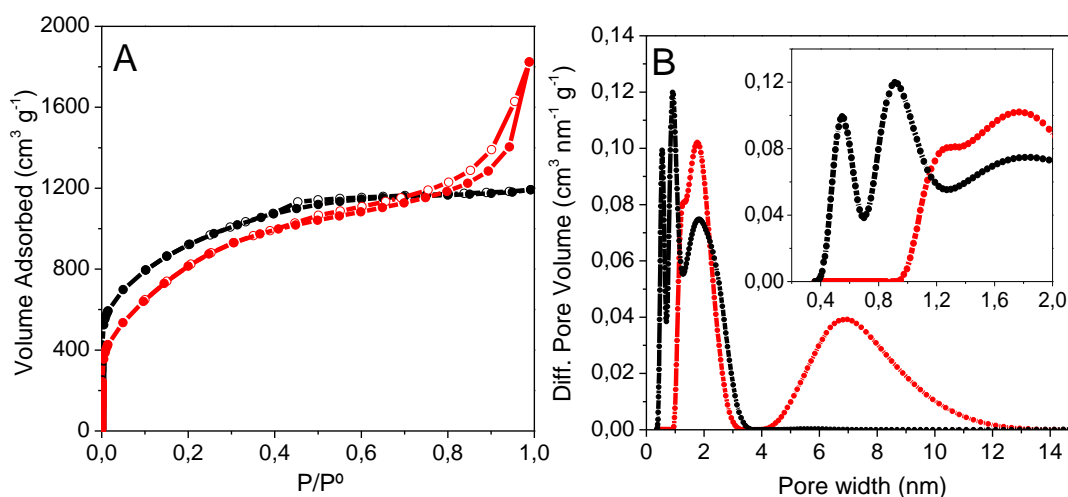
Figure 1. (A) Nitrogen adsorption-desorption isotherms and (B) pore size distributions of MTK (red) and MTKN (black).

Table 1. Textural parameters of the MTK and MTKN activated carbons.

	S_{BET} $(m^2 g^{-1})$	V_T $(cm^3 g^{-1})$	V_{DR} $(cm^3 g^{-1})$	V_{me} $(cm^3 g^{-1})$
MTK	3068	2.82	1.00	1.82
MTKN	3301	1.84	1.13	0.72

S_{BET}, BET specific surface area; V_T, total volume of pores; V_{DR}, micropore volume; V_{me}, mesopore volume.

The morphology of the MTK and MTKN carbons was examined by SEM and TEM. SEM images (Figures 2A and 2C) clearly show that both carbons have different microstructures. MTK shows rougher surface formed by irregularly-shaped carbon vesicles of approximately 50 nm in size.

The inter-particle voids are responsible for the high content of mesopores in this sample (1.82 cm^3 g^{-1}), which provides the MTK carbon with a kind of hierarchical porosity at different length scales. On the other hand, MTKN shows smooth surface with some spherical voids of ca. 2-3 μm in diameter that cannot be measured by nitrogen adsorption. TEM images collected for these carbons at much higher magnification show in both cases the presence of worm-like nanopores randomly distributed in the materials (Figures 2B and 2D). Larger micropores can be clearly identified in the MTK carbon, which is in agreement with the results from the nitrogen adsorption experiments.
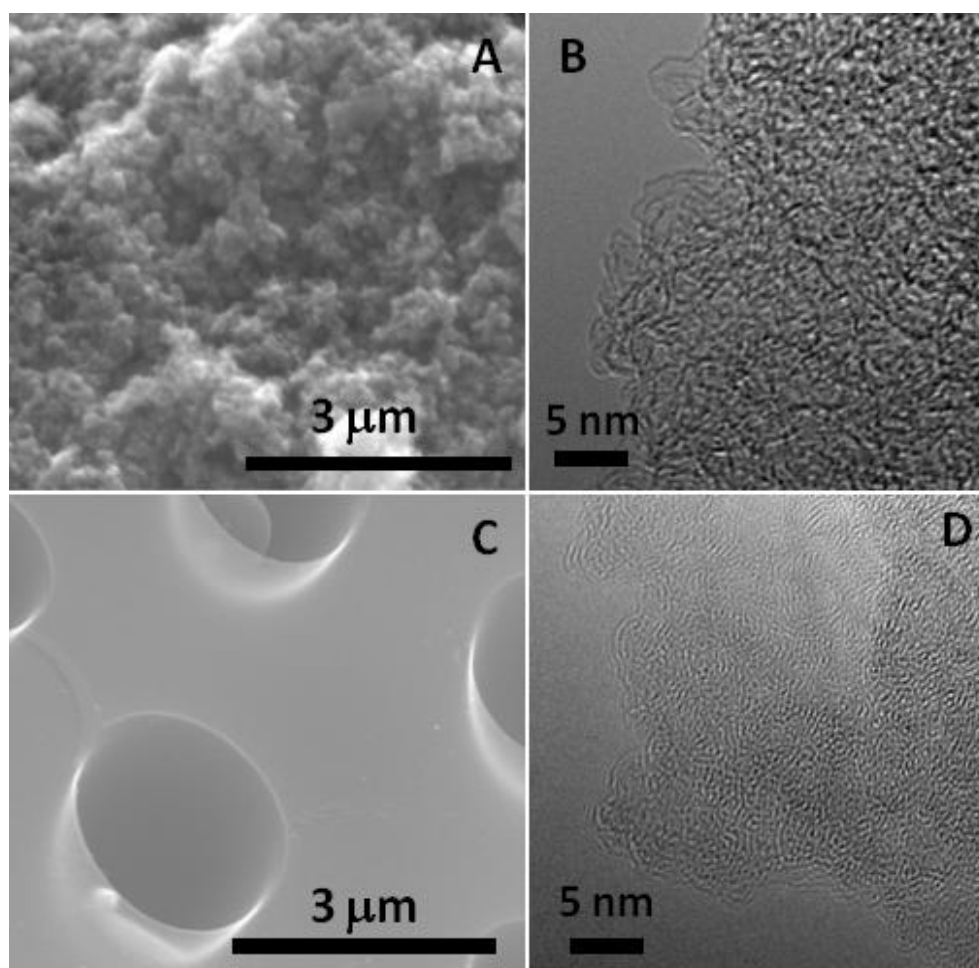
Figure 2. SEM and TEM images of MTK (A and B) and MTKN (C and D) carbons.

The different microstructures observed in the activated carbons must be ascribed to the different effects induced by the different activating agents during the *all-in-one* process. In the

case of the mixture of monomers with KOH, first the polymerization of melamine and terephthaldehyde occurs, followed by the melting of the KOH, the carbonization and the activation of the polymer-derived char by the KOH. On the other hand, the eutectic mixture formed by KOH and NaOH melts at a temperature lower than that of the polymerization of the monomers (ca. 170 ºC). In this latter case, the polymerization presumably took place in a liquid medium, and the polymeric material could have entrapped drops of the eutectic mixture or generated bubbles by the release of reaction products, leaving in the carbonized material the macroscopic spherical voids observed by SEM. Recent works describing the preparation of porous carbons from melamine-terephthaldehyde using molten salts based on LiCl or $ZnCl_2$ with KCl, also ascribed the different morphologies observed to the eutectic liquid media where the polymerizations took place.[31, 32]

The thermal study of the mixture of melamine terephthaldehyde precursors alone and in the presence of the activating agents was performed with the view to getting insight into the effects that the addition of KOH or the KOH + NaOH mixture may have on the polymerization-carbonization-activation processes. Thermogravimetric (TG) and differential thermal analysis (DTA) curves registered for these three systems (melamine + terephtahldehyde, melamine + terephtahldehyde + KOH and melamine + terephtahldehyde + KOH +NaOH) are included in Figure S1. The TG curves of the mixtures with KOH and KOH-NaOH overlap, which indicates similar mechanisms responsible for the weight loss during the one-pot processes. This suggests that the discrepancies in the microstructure of the activated chars are rather influenced by the physical state of the activating agent during the polymerization. As expected, a more intense endothermic process at temperatures below 200 ºC was identified in the presence of the eutectic mixture, according to its low melting point. It should be remarked that the endothermic process registered at 346ºC in the physical mixture of the monomers, which is ascribed to a significant evolution of unreacted melamine, is vanished when the mixture of monomers is heated in presence of the activating agents. Thus, the presence of activating

agents provides a favorable reaction media for the in-situ polymerization compared to the hydroxide-free process. At temperatures over 600ºC, a progressive weight loss is ascribed to the carbonization of the polymer. When the activating agents are present, activation of the carbons also contributes to the weight loss, as confirmed by the endothermic events observed at high temperatures.

X-ray diffraction (XRD) patterns registered for MTK and MTKN carbons are plotted in Figure 3A. The (002) peak related to the periodicity along the z-axis in the hexagonal *ABAB* close packing of graphite structures is absent in both diffraction patterns. This together with the high intense scattering peak at low 2θ values confirms a disordered carbon structure with a very low stacking order of graphene sheets due to the extensive micropore formation during the activation process.[33] Raman spectra (Figure 3B) registered for both samples show peaks centered at 1350 and 1583 cm^{-1}, which correspond to the D and G bands, associated with the existence of defects or edges on disordered carbon and to ordered sp^2 bonded carbon, respectively.[34, 35] The spectra are characteristic of samples formed by amorphous carbon walls containing a large concentration of defects and/or pores, which is in agreement with the XRD measurements.
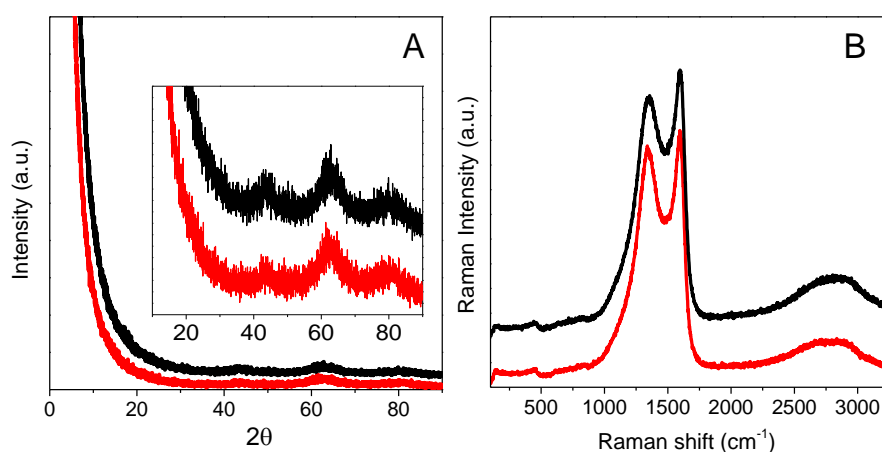

Figure 3. XRD patterns (A) and Raman spectra (B) registered for MTK (red) and MTKN (black) samples.

The high specific surface areas measured for these carbons makes them promising candidates to be used as electrodes in EDLCs. Their electrochemical performances were evaluated using three different aqueous electrolytes: 6M KOH, 1M Li_2SO_4 and 5M LiTFSI. The appropriate voltage window must be chosen for each electrolyte in order to test these carbons in the optimum electrochemical conditions providing for stable cycle life. A voltage window of 1.2 V was considered to test the cells in 6M KOH. In the case of 1M Li_2SO_4 and 5M LiTFSI aqueous solutions, the voltage window was selected based on the CV curves registered at 5 mV s^{-1} for the MTK carbon at increasing voltage ranges (Figure S2). It has been previously reported that these electrolytes allow charging and discharging of the cells at voltage windows as high as 2.2 and 2.4 V for Li_2SO_4 and LiTFSI, respectively.[26, 27] However, according to our CV experiments we decided to limit the voltage window to 1.8 and 2.2 V for Li_2SO_4 and LiTFSI, respectively. It can be noticed that within these voltage window the CV curves exhibit a quasi-rectangular profile and do not show evidence of severe electrolyte decomposition.

The electrochemical performance of symmetric cells using MTK and MTKN electrodes and the three different electrolytes was evaluated by cyclic voltammetry and galvanostatic charge/discharge cycling (Figures 4 and 5, respectively). CV curves of MTK and MTKN in 6M KOH recorded at 10 and 500 mV s^{-1} overlap in the whole voltage range regardless of the sweep rate (Figure 4A and D). It is worth remarking the good retention of the rectangular-shaped profile and the capacitance values of both samples even at a fast scan rate of 0.5 V s^{-1}. Indeed, galvanostatic charge-discharge curves recorded for these systems at a constant current density of 10 A g^{-1} (Figure 5A) exhibit a quasi-linear voltage increase/decrease both at the charge and discharge, which confirms that the storage mechanism is strictly due to the double-layer formation.[36] Specific capacitance values as high as 360 and 330 F g^{-1} (corresponding to cell capacitances of 90 and 82.5 F g^{-1}) were measured at 0.1 A g^{-1} for MTKN and MTK, respectively. The small differences found between these values can be attributed to the slightly larger specific surface area of MTKN compared to MTK. Outstanding capacity retention was observed

for these systems, and high capacitance values of 224 and 221 F g^{-1} were retained at a high current density of 50 A g^{-1} by MTKN and MTK, respectively (Figure 5D).
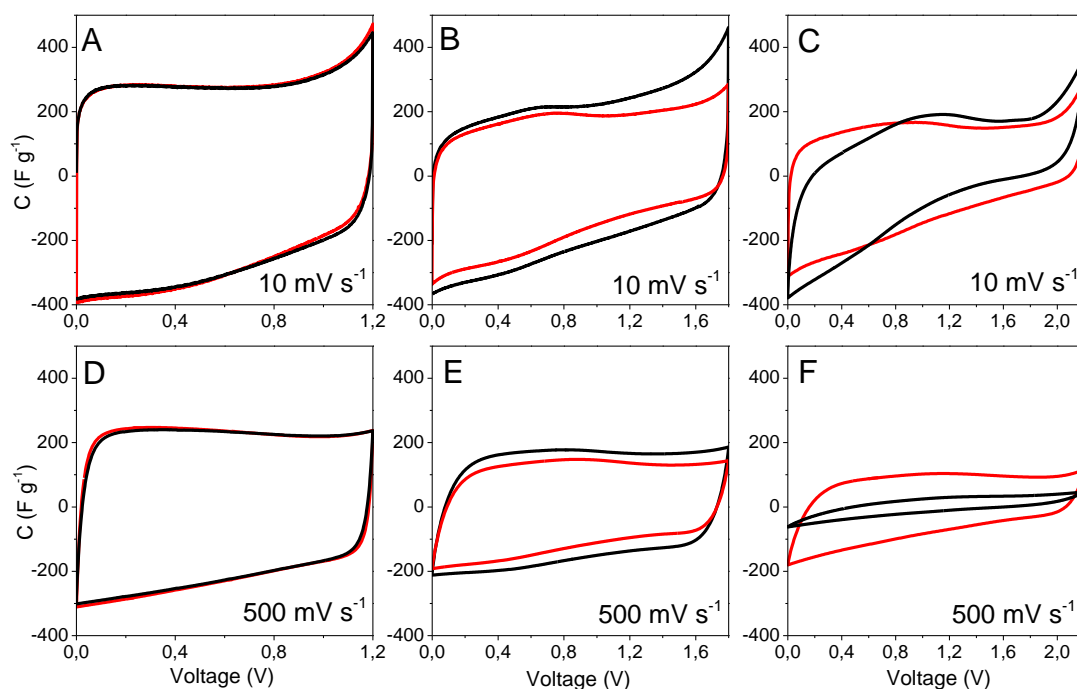
Figure 4. Cyclic voltammograms recorded at 10 and 500 mV s^{-1} for the MTK (red) and MTKN (black) supercapacitors using three different aqueous electrolytes: 6M KOH (A and D), 1M Li$_2$SO$_4$ (B and E) and 5M LiTFSI (C and F).

CV curves registered for MTK and MTKN in 1M Li$_2$SO$_4$ are shown in Figure 4B and 4E. A rectangular-shaped profile characteristic of the EDLC mechanism was also identified, but are slightly distorted, especially for strictly microporous carbon MTKN. The increasing current above ≈1.23V can be due to additional reversible storage of nascent hydrogen in the negative electrode, which is known to be especially noticeable in carbons with a high share of small micropores[37]. At both low and high scan rates, the normalized area under the CV curve is slightly larger in the case of MTKN. Different profiles were also observed in the galvanostatic charge-discharge curves at 10 A g^{-1} (Figure 5B). The discharge branch for MTK shows straight

profile while MTKN exhibits a slight slope change featuring a redox process. This behavior together with the higher capacitance values of MTKN measured both by CV and GC experiments suggest that additional faradaic storage mechanism such as above mentioned hydrogen storage takes place for this sample. Specific capacitance values of 224 and 184 F g^{-1} at a current density of 0.2 A g^{-1} were calculated for the MTKN and MTK carbons, respectively (Figure 5D). These systems displayed good capacitance retention at high current densities, and capacitance values of 144 and 113 F g^{-1} were reached by MTKN and MTK, respectively, at a current density of 50 A g^{-1}.
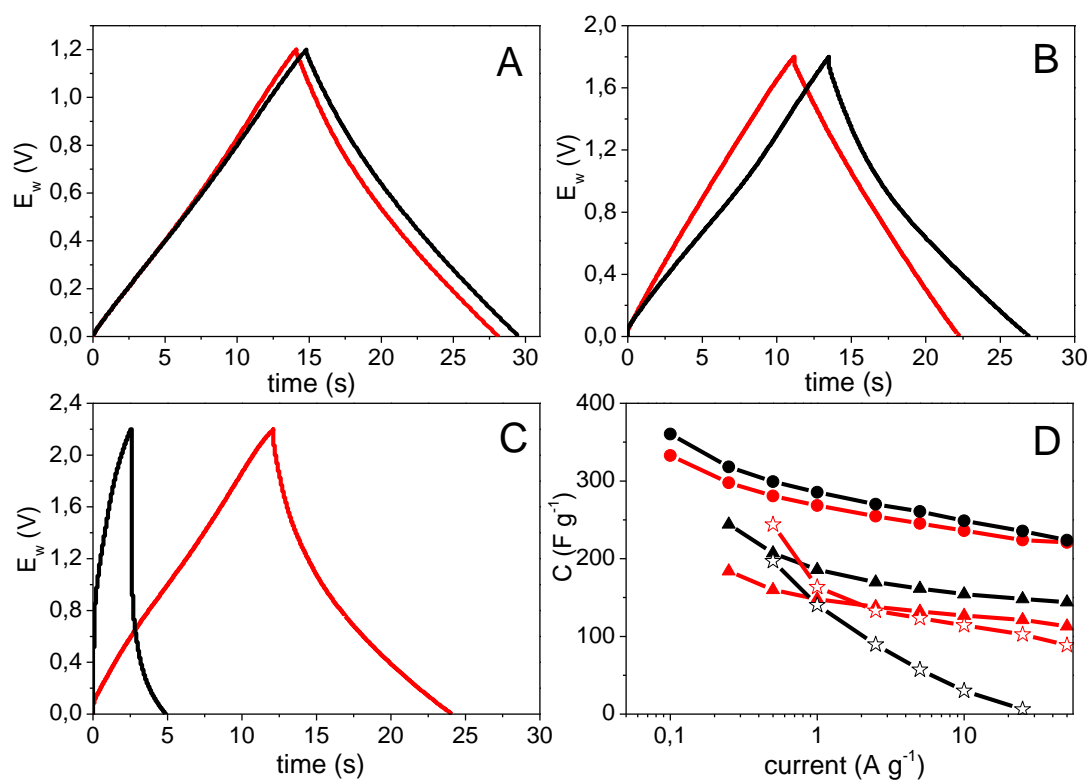

Figure 5. Galvanostatic Charge-Discharge registered at 10 A g^{-1} for the samples MTK (red) and MTKN (black) using different aqueous electrolytes (6M KOH (A, circles), 1M Li$_2$SO$_4$ (B, triangles) and 5M LiTFSI (C, stars)) and specific capacitance evolution vs. Current densities of both samples in different electrolytes.

CV curves registered at 10 mV s^{-1} for MTK and MTKN in 5M LiTFSI exhibit irregular profiles, containing humps and low intense peaks in the voltage limits (Figure 4C). The humps for both

samples can be ascribed to some ion-sievieng effect for the big ions of LiTFSI. For the MTKN sample, the distortion of CV curves at the beginning of charge can arise due to the hindered penetration of the electrolyte deep down micropores, which are smaller than those of MTKN. The MTK sample exhibits a more rectangular profile ensured by its high mesoporosity (see Table 1 and Fig. 1), alleviating the difficulty of electrolyte access to the inner microporosity in comparison to mesopore-free MTKN. As seen in Figure 4F, at a fast sweep rate of 0.5 V s^{-1}, both profiles turn to a more rectangular shape and the peaks are no longer observed. Taking into account the area under the CV curves, it can be glimpsed that MTK has a much higher specific capacitance using LiTFSI as electrolyte compared to MTKN, especially at high-current conditions. Galvanostatic experiments in the 0 to 2.2 V voltage range revealed a strong capacitance decay at increasing current densities. While specific capacitance values over 200 F g^{-1} were measured for both carbons at low current densities (Figure 5D), these values decreased to 140 and 25 F g^{-1} for MTK and MTKN, respectively, at a current of 10 A g^{-1}. Especially, the poor capacitance retention of MTKN is probably related to its porous texture. It has been reported that carbons containing exclusively narrow micropores are not the best candidates for high-power applications due to the restricted ion diffusion within these narrow pores, leading to poor rate capability and power density values.[38] In fact, a large resistance drop was observed in the case of the MTKN (Figure 5C). This is consistent with the current transient in cyclic voltammetry for MTKN as discussed above. On the other hand, it seems that the hierarchical porous structure of the MTK sample is beneficial for the ion diffusion, assuring the better capacitance retention when the cell is cycled at high current densities. Electrochemical impedance spectroscopy measurements corroborate the results from CV and GC experiments. Nyquist plots of MTK and MTKN using 6 M KOH as electrolyte showed vertical lines that overlap along the whole frequency range, characteristic of a purely capacitive system with very low electrical resistance and fast ion diffusion (Figure 6A). When 1M Li$_2$SO$_4$ or 5M LiTFSI were used as the electrolyte, a semicircle was registered at high frequency values,

evidencing the presence of charge transfer processes between the electrode and the electrolyte (Figure 6B and C). In these two latter cases, the presence of 45º slope region at middle frequencies (the de Levie porous electrode factor) also indicates slower ion diffusion due to the bigger size of the electrolyte ions.[39] These features are more clearly observed in the case of mesopore-free MTKN having a narrower micropore size distribution. This fact, combined with the bigger ion size in the Li_2SO_4 and specially 5M LiTFSI electrolytes, may cause some sieving effect and diffusion problems in the porous surface of the electrodes as already mentioned for the cyclic voltammetry data. Relaxation time constants –discharge time at which the ratio of usable-to-lost energy is 50 %– were determined from the EIS data as shown in Figure 6D-F. Extremely small τ_0 values of 0.26 and 0.36 s were calculated from the EIS data for the MTK and MTKN in KOH, respectively. A noticeable increase of this parameter to 1.11 and 1.25 s was identified for the MTKN sample operating in Li_2SO_4 and LiTFSI, respectively. On the other hand, the relaxation time constants of MTK-based SCs were always lower compared to that of MTKN, regardless of the electrolyte used. This reveals a faster response in the case of MTK that must be associated with the hierarchical distribution of the porosity in this sample.[40]

Despite having a smaller total surface area compared to MTKN, the MTK carbon achieved higher capacitance and faster response in 5M LiTFSI. Although this electrolyte allows a wider operating voltage window, it undoubtedly requires electrodes with tuned surface porosities. The presence of a well-developed porous structure both in the micro-and mesoporous range, as determined from the adsorption data, clearly favored a fast diffusion of the electrolyte ions throughout the pore volume of the MTK carbon. In this latter case, it should be also highlighted that the τ_0 value measured using LiTFSI as electrolyte is still similar to that reported for activated carbons based micro-supercapacitors.[23] Therefore, apart from traditional EDLC applications such as hybrid transport vehicles, the MTK material can also be efficient in microdevices, even using low-conductivity electrolytes such as concentrated aqueous LiTFSI.
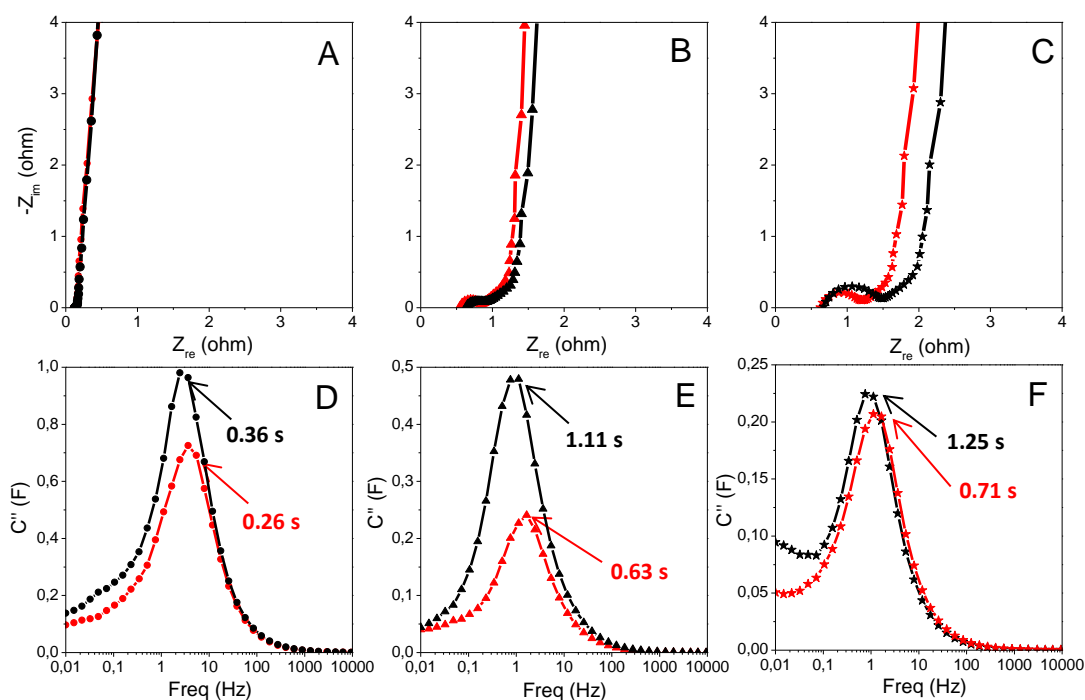
Figure 6. Electrochemical impedance spectroscopy plots. Nyquist plots (A, B and C) and C´´ from Bode plots (D, E and F) registered for MTK (red) an MTKN (black lines) in three different electrolytes: KOH (A and D), Li2SO4 (B and E) and LiTFSI (C and F).

Ragone plots representing the gravimetric energy versus the power density of the cells using MTK and MTKN in the three different aqueous electrolytes are included in Figure 7. The curves were calculated taking into account only the masses of both electrode materials. As expected, higher energy values were achieved for higher operational voltages. In the case of the MTK sample, energy density values of 14, 17 and 40 Wh kg^{-1} were obtained at ca. 0.27 kW kg^{-1} for KOH, Li_2SO_4 and LiTFSI electrolytes, respectively. In the case of MTKN, gravimetric energy values of ca. 14, 22 and 32 Wh kg^{-1} were obtained at the same power density when KOH, Li_2SO_4 and LiTFSI electrolytes were used, respectively. The curves of all the systems, with the exception of MTKN in LiTFSI, merge together in the high power range, achieving an energy density of ca. 10 Wh kg^{-1} at a power density of ca. $2 \cdot 10^4$ W kg^{-1}. The strong failure of MTKN at high power densities using LiTFSI as electrolyte are ascribed to its narrow pore size

distribution, which limits the delivery of energy at short discharge time due to diffusion restrictions as discussed above.
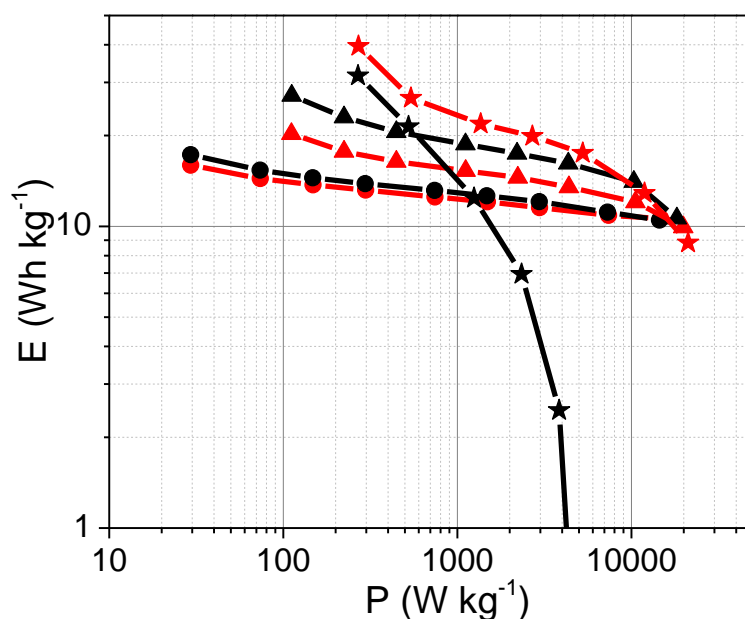

Figure 7. Ragone plot showing the gravimetric energy density versus the gravimetric power density of MTK (red) and MTKN (black) in the three different electrolytes: KOH (circles), Li_2SO_4 (triangles) and LiTFSI (stars) taking into account only the masses of the two electrodes.

Selected samples that exhibited the best performance in the different electrolytes were cycled at 10 A g^{-1} for 10^4 cycles. As shown in Figure 8, MTKN could be steadily cycled in 6M KOH and a very good retention of 91% of the initial capacitance was retained after 10^4 cycles. Interestingly, the MTKN sample tested using Li_2SO_4 as electrolyte showed a progressive increase in the specific capacitance during the first 700 cycles, reaching a specific capacitance value of 230 F g^{-1}. This phenomenon, already reported for other supercapacitor systems,[41-43] can be attributed to the progressive access to some micropores upon cycling that initially were inaccessible and/or a partial pseudocapacitance contribution within these first cycling steps. Further cycling produces a progressive decrease in the specific capacitance, which is still above the initial specific capacitance after 10^4 cycles. This slight activation was not observed for the

MTK sample (figure S3), probably due to its larger micropores and their hierarchical pore size distribution in this sample. The cell built with MTK and LiTFSI maintained a 58% of its initial capacitance after 10^4 cycles, being this capacitance decay probably due to the harsh operating conditions that induces the partial decomposition of the electrolyte.
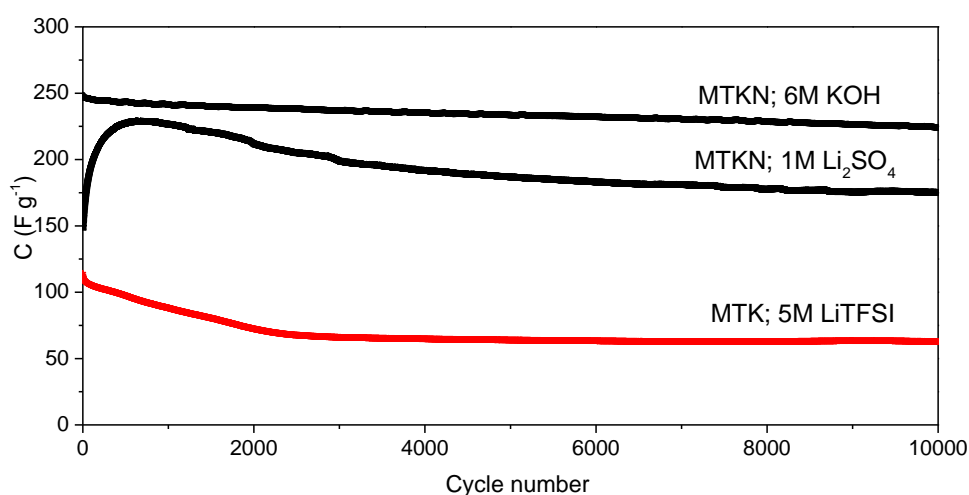
Figure 8. Cycling performance of some selected samples in the indicated electrolytes at 10 A g^{-1}.

Conclusions

In this work an all-in-one procedure for the preparation of high specific surface area carbons with two different textural properties has been presented. The polymerization of melamine and terephthaldehyde in the presence of a eutectic mixture formed by KOH and NaOH allowed obtaining a carbon (MTKN) with a very narrow pore size distribution and SSA of 3300 m^2 g^{-1}, while the carbon obtained only in the presence of KOH (MTK) showed SSA over 3000 m^2 g^{-1} with a hierarchical pore distribution in the micro- and mesopore ranges.

Both MTK and MTKN carbons showed very good performance as electrodes for supercapacitors using 6M KOH as electrolyte. Specific capacitance values over 250 F g^{-1} were achieved by these materials even at a high current density of 10 A g^{-1}, which in terms of energy and power density corresponds to ~ 10 Wh kg^{-1} at 15 kW kg^{-1}, and over 90% of the initial capacitance was retained after 10^4 charge/discharge cycles. Both MTK and MTKN can provide a

very fast response working in 6M KOH, being suitable for high power applications subjected to long cycling.

The electrochemical performance of MTK and MTKN carbons was also assessed using less conventional aqueous electrolyte such as Li_2SO_4 and LiTFSI that allowed increasing the operational voltage window above the thermodynamic stability of water (> 1.23 V). At low values of power density, a very high energy density of 40 Wh kg^{-1} was provided by MTK in LiTFSI. This good performance of MTK in LiTFSI was ascribed to its hierarchical micro-mesoporosity that favored the diffusion of the electrolyte ions. For moderate energy and power requirements, MTKN in Li_2SO_4 can provide 20 Wh kg^{-1} at 1 kW kg^{-1}, which are maintained for at least 10^4 cycles.

Further experiments regarding mass balance in asymmetric cells are under-way to increase the performance and stability of these carbons working in neutral aqueous electrolytes at extended voltage windows.

References

(1) Conway B.E. *Electrochemical capacitors. Scientific fundamentals and technological applications*, Kluwer Academic, New York, **1999**

(2) P. Simon, P.; Gogotsi, Y. Materials for electrochemical capacitors. *Nat. Mater.*, **2008**, 7, 845.

(3) Kötz, R.; Carlen, M. Principles and applications of electrochemical capacitors. *Electrochim. Acta*, **2000**, 45, 2483.

(4) Zhang, L. L.; Zhao, X. S. Carbon-based materials as supercapacitor electrodes. *Chem. Soc. Rev.*, **2009**, 38, 2520.

(5) Lee, J.; Kim, J.; Hyeon, T. Recent Progress in the Synthesis of Porous Carbon Materials. *Adv. Mater.*, **2006**, 18, 2073.

(6) Gu, W.; Yushin, G. Review of nanostructured carbon materials for electrochemical capacitor applications: advantages and limitations of activated carbon, carbide-derived carbon, zeolite-templated carbon, carbon aerogels, carbon nanotubes, onion-like carbon, and graphene. *WIREs Energy Environ.*, **2014**, 3, 424.

(7) Wang, J.; Kaskel, S. KOH activation of carbon-based materials for energy storage. *J. Mater. Chem.*, **2012**, 22, 23710.

(8) Sevilla, M.; Mokaya, R. Energy storage applications of activated carbons: supercapacitors and hydrogen storage. *Energy Environ. Sci.*, **2014**, 7, 1250.

(9) Wei, L.; Sevilla, M.; Fuertes, A. B.; Mokaya, R.; Yushin, G. Hydrothermal Carbonization of Abundant Renewable Natural Organic Chemicals for High-Performance Supercapacitor Electrodes. *Adv. Energy Mater.*, **2011**, 1, 356.

(10) Rufford, T. E.; Hulicova-Jurcakova, D.; Zhu, Z.; Lu, G. Q. Nanoporous carbon electrode from waste coffee beans for high performance supercapacitors. *Electrochem. Commun.*, **2008**, 10, 1594.

(11) Li, Z.; Zhang, Z. L.; Amirkhiz, B. S.; Tan, X. H.; Xu, Z. W.; Wang, H. L.; Olsen, B. C.; Holt, C. M.; Mitlin, D. Carbonized Chicken Eggshell Membranes with 3D Architectures as High-Performance Electrode Materials for Supercapacitors. *Adv. Energy Mater.*, **2012**, 2, 431.

(12) Redondo, E.; Carretero-Gonzalez, J.; Goikolea, E.; Segalini, J.; Mysyk, R. Effect of pore texture on performance of activated carbon supercapacitor electrodes derived from olive pits. *Electrochim. Acta*, **2015**, 160, 178.

(13) Wei, L.; Sevilla, M.; Fuertes, A. B.; Mokaya, R.; Yushin, G. Polypyrrole-Derived Activated Carbons for High-Performance Electrical Double-Layer Capacitors with Ionic Liquid Electrolyte. *Adv. Funct. Mater.*, **2011**, 22, 827.

(14) Guo, S.-L.; Wang, F.; Chen, H.; Ren, H.; Wang, R.; Pan, X. Preparation and performance of polyvinyl alcohol-based activated carbon as electrode material in both aqueous and organic electrolytes. *J. Solid State Electrochem.*, **2012**, 16, 3355.

(15) Ruiz, V.; Pandolfo, A. G. High-frequency carbon supercapacitors from polyfurfuryl alcohol. *J. Power Sources*, **2011**, 196, 7816.

(16) Feng, D.; Lv, Y.; Wu, Z.; Dou, Y.; Han, L.; Sun, Z.; Xia, Y.; Zheng, G.; Zhao, D.-Y. Free-standing mesoporous carbon thin films with highly ordered pore architectures for nanodevices. *J. Am. Chem. Soc.*, **2011**, 133, 15148.

(17) Carriazo, D.; Picó, F.; Gutiérrez, M. C.; Rubio, F.; Rojo, J. M.; del Monte, F. Block-Copolymer assisted synthesis of hierarchical carbon monoliths suitable as supercapacitor electrodes. *J. Mater. Chem.*, **2010**, 20, 773.

(18) Xia, K.; Gao, Q.; Jiang, J.; Hu, J. Hierarchical porous carbons with controlled micropores and mesopores for supercapacitor electrode materials. *Carbon*, **2008**, 46, 1718.

(19) Fang, B.; Kim, J. H.; Kim M.-S.; Yu, J.-S. Hierarchical Nanostructured Carbons with Meso–Macroporosity: Design, Characterization, and Applications. *Acc. Chem. Res.*, **2013**, 46, 1397.

(20) Weinstein, L.; Dash, R. Supercapacitor carbons. *Mater. Today*, **2013**, 16, 356.

(21) Pan, H.; Li, J.; Feng, Y. P. Carbon Nanotubes for Supercapacitor. *Nanoscale Res. Lett.*, **2010**, 5, 654.

(22) Zhu, Y.; Murali, S.; Stoller, M. D.; Ganesh, K. J.; Cai, W.; Ferreira, P. J.; Pirkle, A.; Wallace, R. M.; Cychosz, K. A.; Thommes, M.; Su, D.; Stach, E. A.; Ruoff, R. S. Carbon-based supercapacitors produced by activation of graphene. *Science*, **2011**, 332, 1537.

(23) Pech, D.; Brunet, M.; Durou, H.; Huang, P.; Mochalin, V.; Gogotsi, Y.; Taberna, P.-L.; Simon, P. Ultrahigh-power micrometre-sized supercapacitors based on onion-like carbon. *Nat. Nanotech.*, **2010**, 5, 651.

(24) Wang, G.; Zhang, L.; Zhang, J. A review of electrode materials for electrochemical supercapacitors. *Chem. Soc. Rev.*, **2012**, 41, 797.

(25) Kim, T. Y.; Lee, H. W.; Stoller, M.; Dreyer, D. R.; Bielawski, C. W.; Ruoff, R. S.; Suh, K. S. High-Performance Supercapacitors Based on Poly(ionic liquid)-Modified Graphene Electrodes. *ACS Nano*, **2011**, 5, 436.

(26) Fic, K.; Lota, G.; Meller, M.; Frackowiak, E. Novel insight into neutral medium as electrolyte for high-voltage supercapacitors. *Energy Env. Sci.*, **2012**, 5, 5842.

(27) Hasegawa, G.; Kanamori, K.; Kiyomura, T.; Kurata, H.; Abe, T.; Nakanishi, K. Hierarchically Porous Carbon Monoliths Comprising Ordered Mesoporous Nanorod Assemblies for High-Voltage Aqueous Supercapacitors. *Chem. Mater.*, **2016**, 28, 3944–3950.

(28) He, M.; Fic, K.; Frackowiak, E.; Novak, P.; Berg, E. J. Ageing phenomena in high-voltage aqueous supercapacitors investigated by in situ gas analysis. *Energy Env. Sci.*, **2016**, 9, 623.

(29) Zhao, C.; Zheng, W. A review for aqueous electrochemical supercapacitors. *Front. Energy Res.*, **2015**, 3, 23.

(30) Sing, K. S. W.; Everett, D. H.; Haul, R. A. W.; Moscou, L.; Pierotti, R.; Rouquerol, J.; Sieminiewska, T. Reporting physisorprion data for gas/solid systems with special reference to the determination of surface area and porosity. *Pure Appl. Chem.,* **1985**, 57, 603.

(31) He, B.; Li, W.-C.; Lu, A.-H. High nitrogen-content carbon nanosheets formed using the Schiff-base reaction in a molten salt medium as efficient anode materials for lithium-ion batteries. *J. Mater. Chem. A*, **2015**, 3, 579.

(32) Su, S.; Lai, Q.; Liang, Y. Schiff-base polymer derived nitrogen-rich microporous carbon spheres synthesized by molten-salt route for high-performance supercapacitors. *RSC Adv.*, **2015**, 5, 60956.

(33) Yun, S.; Cho, S. Y.; Shim, J.; Kim, B. H.; Chang, S.-J.; Baek, S. J.; Huh, Y. S.; Tak, Y.; Park, Y. W.; Park S.; Jin, H.-J. Microporous carbon nanoplates from regenerated silk proteins for supercapacitors. *Adv. Mater.*, **2013**, 25, 1993.

(34) Carriazo, D.; Gutiérrez, M. C.; Jiménez, R.; Ferrer, M. L.; del Monte, F. Deep-eutectic-assisted synthesis of bimodal porous carbon monoliths with high electrical conductivities. *Part. Part. Syst. Charact.*, **2013**, 30, 316.

(35) Tarrant, R.N.; Warschkow, O.; McKenzie, D.R. Raman spectra of partially oriented sp^2 carbon films: Experimental and modeled. *Vib. Spectrosc.*, **2006**, 41, 232.

(36) Wang, Y.; Song, Y.; Xia, Y. Electrochemical capacitors: mechanism, materials, systems, characterization and applications. *Chem. Soc. Rev.*, **2016**, 45, 5925.

(37) Vix-Guterl, C.; Frackowiak, E.; Jurewicz, K.; Friebe, M.; Parmentier, J.; & Béguin, F. Electrochemical energy storage in ordered porous carbon materials. *Carbon*, **2005**, 43, 1293.

(38) Chmiola, J.; Yushin, G.; Dash, R.; Gogotsi, Y. Effect of pore size and surface area of carbide derived carbons on specific capacitance. *J. Power Sources*, **2006**, 158, 765.

(39) Taberna, P. L.; Simon, P.; Fauvarque, J. F. Electrochemical characteristics and impedance spectroscopy studies of carbon-carbon supercapacitors. *J Electrochem. Soc.*, **2003**, 150, A292-A300.

(40) Ferrero, G. A.; Fuertes, A. B.; Sevilla, M. From Soybean residue to advanced supercapacitors. *Sci. Reports*, **2015**, 5, 16618.

(41) Hastak, R.S.; Sivaraman, P.; Potphode, D.D.; Shashidhara, K.; Samui, A.B. All solid supercapacitor based on activated carbon and poly [2,5-benzimidazole] for high temperature application. *Electrochim. Acta*, **2012**, 59, 296.

(42) Lin, H.; Li, L.; Ren, J.; Cai, Z.; Qiu, L.; Yang, Z.; Peng, H. Conducting polymer composite film incorporated with aligned carbon nanotubes for transparent, flexible and efficient supercapacitor. *Sci. Reports*, **2013**, 3, 1353.

(43) Hahn, M.; Barbieri, O.; Gallay, R.; Kötz, R. A dilatometric study of the voltage limitation of

carbonaceous electrodes in aprotic EDLC type electrolytes by charge-induced

strain. *Carbon*, **2006**, 44, 2523.

One-Pot Synthesis of Activated Carbons from Melamine Terephthaldehyde as

Electrodes for High Energy Aqueous Supercapacitors

Noel Díez,[a] Roman Mysyk,[a] Wei Zhang,[ab] Eider Goikolea,[a] Daniel Carriazo *[ab]
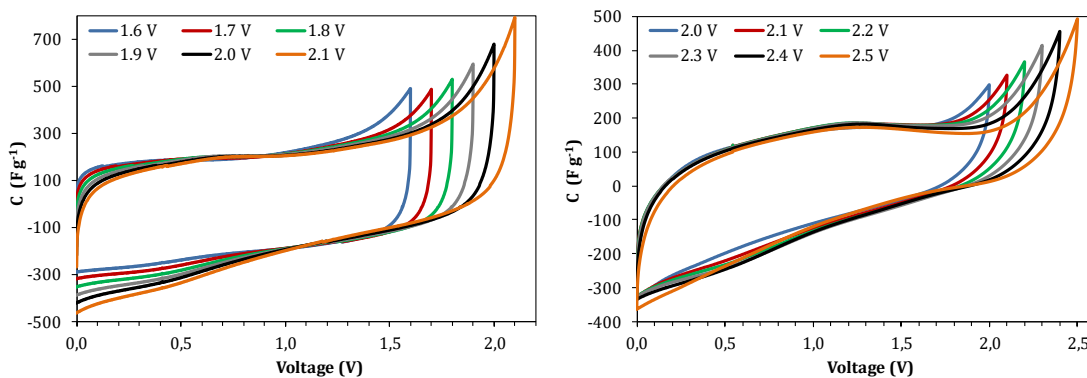
[a] CIC EnergiGUNE, Parque Tecnológico de Álava, Albert Einstein 48, 01510 Miñano, Álava, Spain

[b] IKERBASQUE, Basque Foundation for Science, 48013 Bilbao, Spain

e-mail: dcarriazo@cicenergigune.com
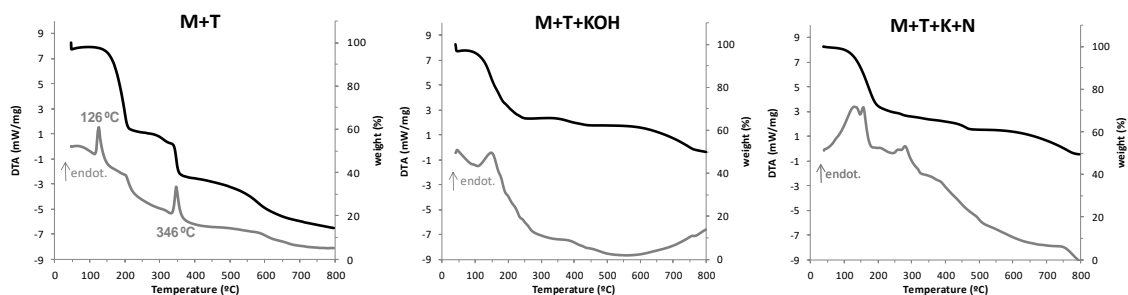
Figure S1. TG and DTA curves registered for the precursors alone and in combination with KOH or NaOH-KOH registered under argon atmosphere with a heating ramp or 5ºC min^{-1}

Figure S2. CV recorded for sample MTK at 5 mV s^{-1} using Li_2SO_4 (A) and LTFSI (B) as aqueous electrolytes.
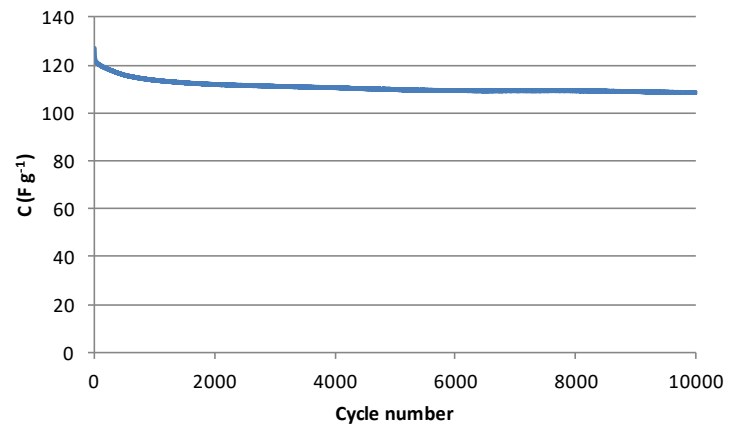
Figure S3. Cycling performance of MTK sample in 1M Li_2SO_4 at 10 A g^{-1}.